JOHANNES KEPLER
UNIVERSITÄT LINZ

Submitted by:
Gerold Volker Kristanz

Advisors:
Prof. Thomas Klar
Prof. Alexander Kildishev

Assistance:
Dr. Nikita Arnold
Dr. Calin Hrelescu

March 2016

Numerical modeling of nonlinearly coupled effects in nanoplasmonic devices

Thermal limitations of a spaser

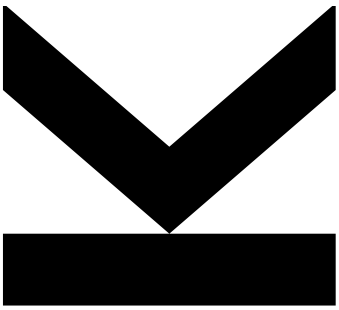

Progress Report

for the

Austrian Marshall Plan Foundation

regarding the stay abroad at

Purdue University

JOHANNES KEPLER
UNIVERSITÄT LINZ
Altenbergerstraße 69
4040 Linz, Österreich
www.jku.at
DVR 0093696

1 Introduction

The field of nanoplasmonics is one of the most dynamic branches of physics in the 21st century. Its current enormous growth is outmatched only by the widespread application of its ideas and concepts. Nanoplasmonic devices such as plasmonically enhanced organic solar cells,[1] organic light emitting diodes[2] or nanoscopic coherent light sources[3] are destined to have a massive impact on future technologies.

My primary task at Purdue University was to simulate full-wave optics of nonlinear media using Maxwell's equations coupled with other partial differential equations (e.g., the heat equation). The term nonlinear media here refers to materials whose optical properties may depend on intensity, as well as other variables like temperature, thus complicating the situation. Due to the high complexity of the problem, simulations of this kind are almost absent in the field of nanoplasmonics.

A very new and promising device in nanoplasmonics is the so-called spaser. First predicted in 2003 by Bergman and Stockman,[4] a spaser basically is a coherent nanoscopic light source. The name itself is an acronym for **s**urface **p**lasmon **a**mplification by **s**timulated **e**mission of **r**adiation, very similar to the commonly known laser (**l**ight **a**mplification...). I focus my efforts on simulating the transient thermal behaviour of such a device. The heating of plasmonic nanostructures is interesting in two different aspects: Either the heating is a desired effect, e. g. for medical applications of nanoparticles in living tissue,[5] or it threatens the realizability of the device. Some spaser types may work perfectly in theory, but vaporize within a microsecond when operating in a continuous mode. Hence, the subtitle of my progress report is: "Thermal limitations of a spaser". In it, I study the maximum range of parameters under which a spaser can still safely operate.

As a test problem to verify different aspects of the used numerical framework, I first consider the electromagnetic heating of a spherical silver nanoparticle. This problem is especially well suited, since it has been extensively studied in literature,[6–13] and it can be solved analytically in very good approximation.

2 Test problem: Electromagnetically heated sphere

2.1 Introduction

In this chapter, I investigate the electromagnetic heating of a small (50 nm radius) silver nanoparticle in an infinite water ambient. The same problem for gold nanoparticles has

Symbol	Definition	Unit
a	Particle radius	m
S	Particle surface, $S = 4\pi a^2$	m^2
V	Particle volume, $V = 4\pi a^3/3$	m^3
$T(r,t)$	Temperature	K
$T_\mathrm{p}(t)$	Particle surface temperature, $T_\mathrm{p}(t) = \lim_{\eta\to 0^+} T(a-\eta,t)$	K
$T_\mathrm{a}(t)$	Ambient surface temperature, $T_\mathrm{a}(t) = \lim_{\eta\to 0^+} T(a+\eta,t)$	K
$\delta T_\mathrm{c}(t)$	Particle core temperature rise, $\delta T_\mathrm{c}(t) = T(0,t) - T_\mathrm{p}(t)$	K
ρ	Density	$\mathrm{kg/m}^3$
c	Specific heat capacity	$\mathrm{J/(kg\,K)}$
k	Thermal conductivity	$\mathrm{W/(m\,K)}$
D	Diffusivity, $D = k/(c\rho)$	m^2/s
G	Kapitza conductance	$\mathrm{W/(m}^2\,\mathrm{K)}$
Q	Heat source	$\mathrm{W/m}^3$
P	Total heating power of the sphere, $P = \int_V d^3x\, Q(\mathbf{x})$	W
$\mathbf{E}$	Electric field	V/m
$\mathbf{k}$	Wave vector (of exciting wave)	m^{-1}

Table 1: A list of the most important physical quantities and material properties appearing in this work.

been extensively studied in literature: Govorov et al. and Richardson et al. investigated melting and heating effects,[7,8] Hu et al. and Stoll et al. described cooling dynamics via pump-probe experiments[9,10] and Harris et al., Richardson et al. and Jiang et al. discuss possibilities for heating optimization.[11–13] Also, Chen et al. solves the identical problem (including Kapitza resistance) numerically for a 50 nm radius gold nanoparticle.[6]

First, I discuss a simplified model, which can be solved analytically. My model is similar to the model of Goldenberg et al.,[14] only I use interfacial thermal (Kapitza) resistance instead of continuity of temperature as boundary condition at the particle-ambient interface. In section 2.3, the problem is numerically solved using finite element techniques.

To achieve a maximum temperature change, the particle is excited at its quadrupolar resonance, which is at 390 nm (see figure 1). For sake of simplicity, I set the initial temperature to zero in this chapter. Table 1 contains all relevant physical quantities. Please note that material constants can be accompanied by a subscript "p" or "a", indicating that they are either particle or ambient properties.

2.2 Analytical model

If a nanoparticle is electromagnetically heated, the heat source $Q \propto |\mathbf{E}|^2$ inside the particle is usually not position-independent. However, since the heat conductivity of silver (or metal in general) is very high, the temperature in the particle will even out very

quickly. Hence, one can model the system with a spatially constant power source.

The particle is surrounded infinitely by an ambient material (e. g. water). To simplify the problem further, I assume all material properties to be temperature-independent and I make use of the spherical symmetry.

The boundary conditions for the flux at the particle-ambient interface are

$$J(a,t) = G\Big(T_\mathrm{p}(t) - T_\mathrm{a}(t)\Big), \tag{1}$$

$$J(a,t) = -k_\mathrm{p} \lim_{\epsilon\to 0^+} \nabla T(r,t)|_{r=a-\epsilon} = -k_\mathrm{a} \lim_{\epsilon\to 0^+} \nabla T(r,t)|_{r=a+\epsilon}. \tag{2}$$

Equation (1) reflects the thermal Kapitza resistance while equation (2) is the continuity of flux. Even though the temperature inside the particle will be almost constant, the former demands a non-zero temperature gradient inside. Hence, I assume a slightly parabolic decrease

$$T(r<a,t) = T_\mathrm{p}(t) + \left(1 - \frac{r^2}{a^2}\right)\delta T_\mathrm{c}(t), \tag{3}$$

where T_p is the surface and $T_\mathrm{p} + \delta T_\mathrm{c}$ the core temperature of the particle. Further, the comparison of equations (2) and (3) yields for δT_c:

$$\delta T_\mathrm{c}(t) = \frac{a}{2k_\mathrm{p}} J(a,t) \tag{4}$$

In the ambient region, the temperature satisfies the heat equation, i. e.

$$\dot{T}(r,t) = D_\mathrm{a} \Delta T(r,t). \tag{5}$$

Substituting $T = u/r$ reduces the problem to a 1D heat equation,

$$\dot{u}(r,t) = D_\mathrm{a} u_{rr}(r,t), \tag{6}$$

where a subscript 'r' denotes the derivative with respect to the radius. This equation can be solved in Laplace space (assuming $u(r,0) = 0$), transforming back and evaluating at $r = a$ yields

$$u(a,t) = -\sqrt{\frac{D_\mathrm{a}}{\pi}} \int_0^t dt' \frac{u_r(a,t')}{\sqrt{t-t'}}. \tag{7}$$

Taking the time derivative and applying an inverse Abel transform yields

$$u_r(a,t) = -\frac{1}{\sqrt{D_\mathrm{a}\pi}} \int_0^t dt' \frac{\dot{u}(a,t')}{\sqrt{t-t'}}, \tag{8}$$

which can be used to express the flux at the boundary

$$J(a,t) = \frac{k_\mathrm{a}}{a} T_\mathrm{a}(t) + \frac{k_\mathrm{a}}{\sqrt{D_\mathrm{a}\pi}} \int_0^t dt' \frac{\dot{T}_\mathrm{a}(t')}{\sqrt{t-t'}}. \tag{9}$$

Inside the particle, the heat equation is

$$c_\mathrm{p}\rho_\mathrm{p}\dot{T}(r,t) = k_\mathrm{p}\Delta T(r,t) + Q. \tag{10}$$

Note that, even on a nanoscopic scale, the heat equation remains valid according to Keblinski et al.[15] Substituting $\dot{T}$ with equation (3) and integrating over the sphere yields

$$P = V c_\mathrm{p}\rho_\mathrm{p}\left(\dot{T}_\mathrm{p}(t) + \frac{2}{5}\delta\dot{T}_\mathrm{c}(t)\right) + SJ(a,t). \tag{11}$$

To further simplify the relevant equations, I introduce reduced units, which are denoted by an asterisk.

$$T(r,t) = T^*(r,t^*)T_\mathrm{st}, \qquad T_\mathrm{st} = \frac{P}{4\pi a k_\mathrm{a}}, \tag{12}$$

$$J(r,t) = J^*(r,t^*)J_\mathrm{st}, \qquad J_\mathrm{st} = P/S, \tag{13}$$

$$t = t^* t_\mathrm{st}, \qquad t_\mathrm{st} = \frac{a^2 c_\mathrm{p}\rho_\mathrm{p}}{3k_\mathrm{a}}. \tag{14}$$

In reduced units, equations (1), (4), (9) and (11) are

$$J^*(a,t^*) = \frac{Ga}{k_\mathrm{a}}(T^*_\mathrm{p}(t^*) - T^*_\mathrm{a}(t^*)), \tag{15}$$

$$\delta T^*_\mathrm{c}(t^*) = \frac{k_\mathrm{a}}{2k_\mathrm{p}} J^*(a,t^*), \tag{16}$$

$$J^*(a,t^*) = T^*_\mathrm{a}(t^*) + \sqrt{\frac{3c_\mathrm{a}\rho_\mathrm{a}}{\pi c_\mathrm{p}\rho_\mathrm{p}}} \int_0^{t^*} d\eta \frac{\dot{T}^*_\mathrm{a}(\eta)}{\sqrt{t^*-\eta}}, \tag{17}$$

$$J^*(a,t^*) = 1 - \dot{T}^*_\mathrm{p}(t^*) - \frac{2}{5}\delta\dot{T}^*_\mathrm{c}(t^*). \tag{18}$$

Please note that in this context $\dot{T}^*$ is the derivative of the reduced temperature with respect to t^*, not t. One can solve these equations in Laplace space, assuming zero initial

temperature and flux,

$$\tilde{T}^*_{\mathrm{p}}(s) = \frac{\sqrt{s} + c^{-1} + gc^{-1}}{(1 + \frac{2}{5}kg)\Delta(s)}, \tag{19}$$

$$\tilde{T}^*_{\mathrm{a}}(s) = \frac{gc^{-1}}{(1 + \frac{2}{5}kg)\Delta(s)}, \tag{20}$$

$$\delta\tilde{T}^*_{\mathrm{c}}(s) = k\tilde{J}^*(a,s) = \frac{kg(\sqrt{s} + c^{-1})}{(1 + \frac{2}{5}kg)\Delta(s)}, \tag{21}$$

$$g = \frac{Ga}{k_{\mathrm{a}}}, \qquad k = \frac{k_{\mathrm{a}}}{2k_{\mathrm{p}}}, \qquad c = \sqrt{\frac{3c_{\mathrm{a}}\rho_{\mathrm{a}}}{c_{\mathrm{p}}\rho_{\mathrm{p}}}}. \tag{22}$$

The common denominator Δ is a fifth degree polynomial in $\sqrt{s}$,

$$\Delta(s) = s(\sqrt{s} + \alpha)(\sqrt{s} + \beta)(\sqrt{s} + \gamma), \tag{23}$$

whose non-trivial roots satisfy

$$c^{-1}(\kappa + 1) = \alpha + \beta + \gamma, \tag{24}$$

$$\kappa = \alpha\beta + \alpha\gamma + \beta\gamma, \tag{25}$$

$$c^{-1}\kappa = \alpha\beta\gamma, \tag{26}$$

$$\kappa = \frac{g}{1 + \frac{2}{5}kg}. \tag{27}$$

For equations (19)-(21) only two essential inverse Laplace transforms are needed,

$$\frac{\sqrt{s}}{\Delta(s)} \bullet\!\!-\!\!\circ \sum_{\substack{s_i \in \{\alpha,\beta,\gamma\} \\ i \neq j \neq k}} \frac{\mathrm{e}^{s_i^2 t^*}\mathrm{erfc}(s_i\sqrt{t^*})}{(s_i - s_j)(s_i - s_k)} := \Sigma_0(t^*), \tag{28}$$

$$\frac{1}{\Delta(s)} \bullet\!\!-\!\!\circ \frac{1}{\alpha\beta\gamma}\left(1 - \sum_{\substack{s_i \in \{\alpha,\beta,\gamma\} \\ i \neq j \neq k}} \frac{s_j s_k \mathrm{e}^{s_i^2 t^*}\mathrm{erfc}(s_i\sqrt{t^*})}{(s_i - s_j)(s_i - s_k)}\right) := \frac{1 - \Sigma_1(t^*)}{\alpha\beta\gamma}. \tag{29}$$

Now equations (19)-(21) can be easily transformed back into real space,

$$T^*_{\mathrm{p}}(t^*) = \frac{\kappa}{g}\Sigma_0(t^*) + \frac{1+g}{g}\Big(1 - \Sigma_1(t^*)\Big), \tag{30}$$

$$T^*_{\mathrm{a}}(t^*) = 1 - \Sigma_1(t^*), \tag{31}$$

$$\delta T^*_{\mathrm{c}}(t^*) = kJ^*(a,t^*) = k\Big(1 + \kappa\Sigma_0(t^*) - \Sigma_1(t^*)\Big), \tag{32}$$

Additionally, one can show that

$$\lim_{t^* \to \infty} T^*_{\mathrm{a}}(t^*) = \lim_{t^* \to \infty} J^*(r,t^*) = 1, \tag{33}$$

thus motivating the names "stationary temperature" and "stationary flux" for T_{st} and J_{st}. However, note that the limit for T_{p}^* is unequal to 1,

$$\lim_{t^*\to\infty} T_{\mathrm{p}}^*(t^*) = 1 + g^{-1}. \tag{34}$$

The general solutions can be simplified, if one assumes a particle with high heat conductivity and no Kapitza resistance. Applying the limits $g \to \infty$ and $k \to 0$, $\Delta(s)$ degenerates into a second degree polynomial in $\sqrt{s}$,

$$\lim_{g\to\infty}\lim_{k\to 0}\Delta(s) = s + c\sqrt{s} + 1. \tag{35}$$

The result for the surface temperature then simplifies to

$$T^*(r=a,t^*) = 1 - \frac{\alpha_2 \mathrm{e}^{\alpha_1^2 t^*}\mathrm{erfc}(\sqrt{\alpha_1 t^*})}{\alpha_2-\alpha_1} - \frac{\alpha_1 \mathrm{e}^{\alpha_2^2 t^*}\mathrm{erfc}(\sqrt{\alpha_2 t^*})}{\alpha_1-\alpha_2}, \tag{36}$$

$$\alpha_{1/2} = \frac{1}{2}\Big(c \pm \sqrt{c^2-4}\Big). \tag{37}$$

2.3 Finite element simulation

I simulate a 50 nm radius silver particle with the dielectric function of Johnson and Christy,[16] which is surrounded by water. According to Mie theory,[17] such a particle has a quadrupolar resonance at 390 nm (see figure 1), hence I choose this as my excitation wavelength. To simulate a realistic scenario, I choose the excitation intensity to be 9550 W/cm^2, which corresponds to a 30 mW laser focused on a circular, 10 μm radius spot.

All thermal and electromagnetic material properties are assumed to be constant, hence the problem is decoupled. I first simulate the field distribution in the particle to calculate a heat source $Q \propto |\mathbf{E}|^2$, which I then insert into the heat equation and solve for the temperature. The used material constants are given in table 2.

2.3.1 Expectations

Mie theory yields an absorption cross section of 0.01754 μm^2 at 390 nm (see figure 1), hence the absorbed power P should be 1.675 μW. This in turn can be used to calculate the transient limit of the particle surface temperature T_{p} (see equation (34)), which yields a total temperature change of approximately 5.02 K.

Name	Symbol	Value for Ag	Value for H_2O
Relative permittivity	$\varepsilon'_r + i\varepsilon''_r$	$-3.8951 + 0.1974i$	1.7951
Relative permeability	$\mu'_r + i\mu''_r$	1	1
Thermal conductivity	k	$430\,\mathrm{W/(m\,K)}$	$0.5942\,\mathrm{W/(m\,K)}$
Density	ρ	$10490\,\mathrm{kg/m^3}$	$999.6\,\mathrm{kg/m^3}$
Specific heat capacity	c	$235\,\mathrm{J/(kg\,K)}$	$4187\,\mathrm{J/(kg\,K)}$
Kapitza conductance	G	$10^8\,\mathrm{W/(m^2\,K)}$	

Table 2: Used material constants for the simulation. Note that thermodynamic quantities are assumed temperature-independent and electrodynamic quantities are given for a wavelength of 390 nm. Also, the given Kapitza conductance is for the silver/water interface, even though it is attributed to silver in the table.

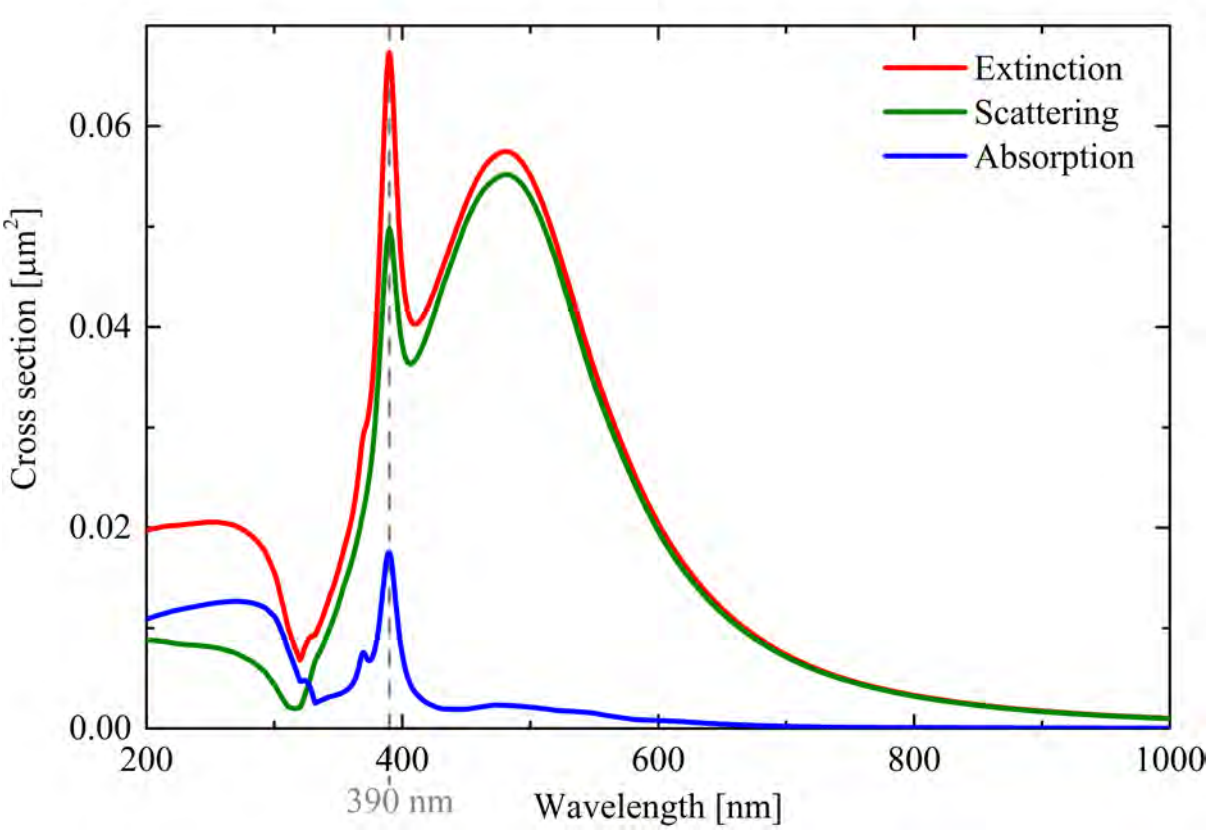

Figure 1: Cross sections for a 50 nm radius Johnson-Christy silver particle surrounded by water according to Mie theory. The gray, dotted line at 390 nm marks the quadrupolar resonance. The calculations have been done with the program *MQMie*.

2.3.2 Boundary condition

The choice of boundary condition is crucial for the accuracy of FEM calculations. In this, it should be chosen as such that all the heat propagates to infinity and none is reflected back to the particle. A reasonable choice is the convection boundary condition, which assumes that, far away from the system, the stationary temperature behaves like for a localized, time-independent source. At the boundary, the flux should satisfy

$$J(\mathbf{x},t)|_{r=R} = \frac{k_\mathrm{a}}{R}\Big(T(\mathbf{x},t)|_{r=R} - T_0\Big), \tag{38}$$

where R is the radius of the computational domain and T_0 the temperature at infinity (usually zero). Mathematically speaking, this condition is called a Robin boundary condition, which is a combination of a Dirichlet and a Neumann boundary condition.

Since this condition in fact imposes the stationary solution on the system, it can lead to unrealistically fast convergence if the computational domain is too small. Hence I also introduce an infinite element domain, which is best described in the COMSOL user manual itself:[18]

> "An Infinite Element Domain [...] applies a rational coordinate scaling to a layer of virtual domains surrounding the physical region of interest. When the dependent variables vary slowly with radial distance from the centre of the physical domain, the finite elements can be stretched in the radial direction such that boundary conditions on the outside of the infinite element layer are affectively applied at a very large distance from any region of interest."

Using an infinite element domain, one could even replace the convection boundary condition with a constant temperature one – the difference is negligible.

2.3.3 Results

Electrodynamic calculation The field distribution $|\mathbf{E}|$ is shown in figure 2 while figure 3 shows the heat source $Q \propto |\mathbf{E}|^2$ inside the particle. Due to high forward scattering, the heat source is highest at the side which is averted from the laser. Also, since the particle diameter is much larger than the skin depth of electromagnetic waves (roughly 10-20 nm for silver at 390 nm wavelength), Q is concentrated near the surface.

One can numerically integrate the heat source over the particle to get the total heating power,

$$P = \int_V d^3x\, Q(\mathbf{x}) \approx 1.658\,\mu\mathrm{W}. \tag{39}$$

This value for P is in agreement with the result obtained via Mie theory in section 2.3.1 – the 1 % deviation probably exists due to the finite mesh. Since the power is an input quantity for the thermal simulation, I use the value given in equation (39) for further calculations rather than the value given in section 2.3.1.

Thermal calculations The results from the thermal simulation agree with the analytical model of chapter 2.2. In figures 7 and 8 the particle and ambient surface temperatures are compared with their analytical counterpart. Although there is difference for very small times, for $t \geq 1\,\mathrm{ns}$ both temperatures coincide. Figure 6 compares the particle and ambient surface temperatures of the simulation. Since there is always a heat flux over the boundary, both temperatures do not converge to the same value, but rather to the limits given in equations (33) and (34).

The given surface temperatures have not been averaged over the particle surface, but instead evaluated at two points on the z-axis ($z = 0.9999a$ and $z = 1.0001a$, see figures 4 and 5). An evaluation directly at the surface would lead to unphysical results, since the temperature jumps due to the Kapitza resistance. One would need to average over two spheres with radii slightly smaller and larger than a. However, since this is very cumbersome, it has been omitted here.

Figure 4 shows the temperature distribution after 100 ps. Since the heat conductivity of silver is three orders of magnitude higher than that of water, the temperature in the sphere is almost constant. From the fundamental solution of the heat equation, one can find that the typical time the temperature needs to spread over the particle is approximately 3.6 ps. The temperature distribution in the system after 2000 ns can be seen in figure 5. The system is very close to thermal equilibrium. Hence, inside the particle the temperature is almost constant while outside it decreases with $1/r$.

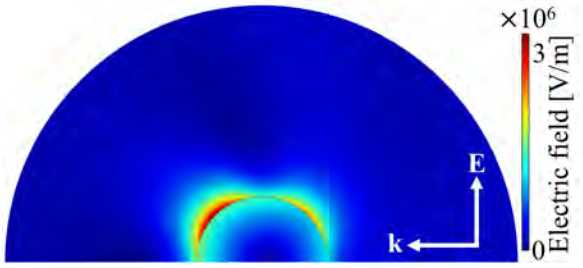

Figure 2: Absolute value of the electric field in the near vicinity of the particle. The arrows denoted with **E** and **k** represent the polarization and wave vector of the exciting wave, respectively.

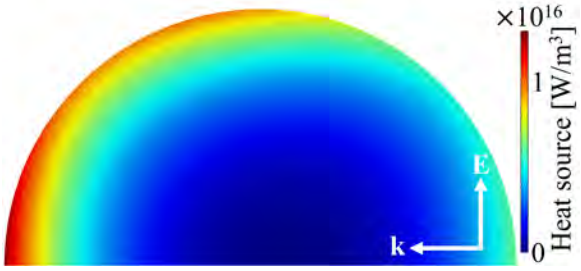

Figure 3: Heat source in the particle. Note that $Q \propto |\mathbf{E}|^2$.

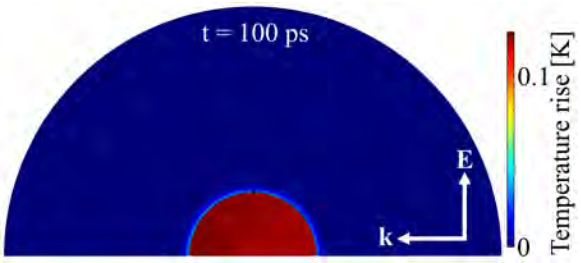

Figure 4: Temperature distribution after 100 ps. The small, black square is the point of evaluation for both surface temperatures, see figures 7 - 6.

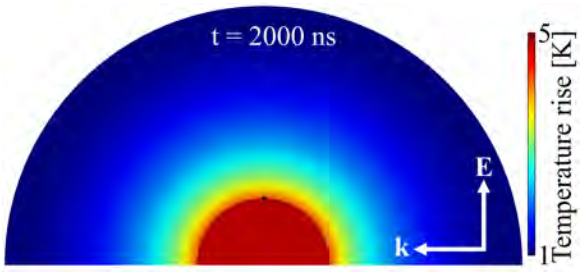

Figure 5: Temperature distribution after 2000 ns.

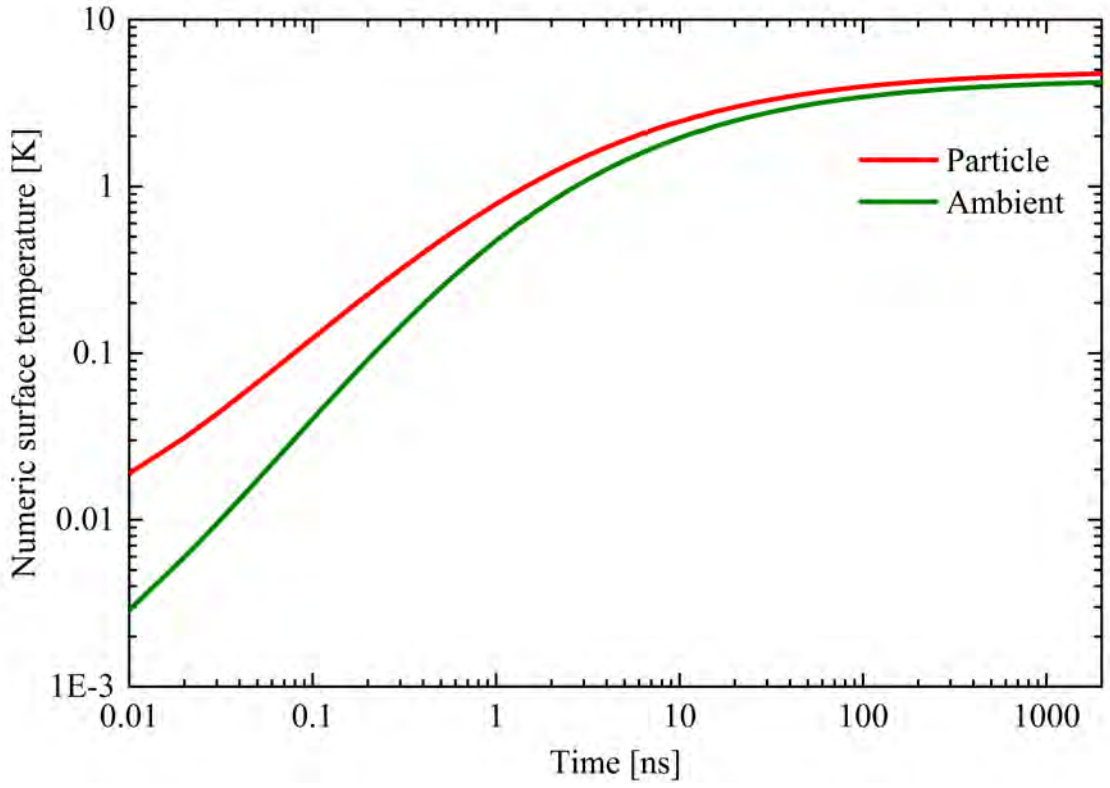

Figure 6: Comparison of the numeric particle and ambient surface temperatures.

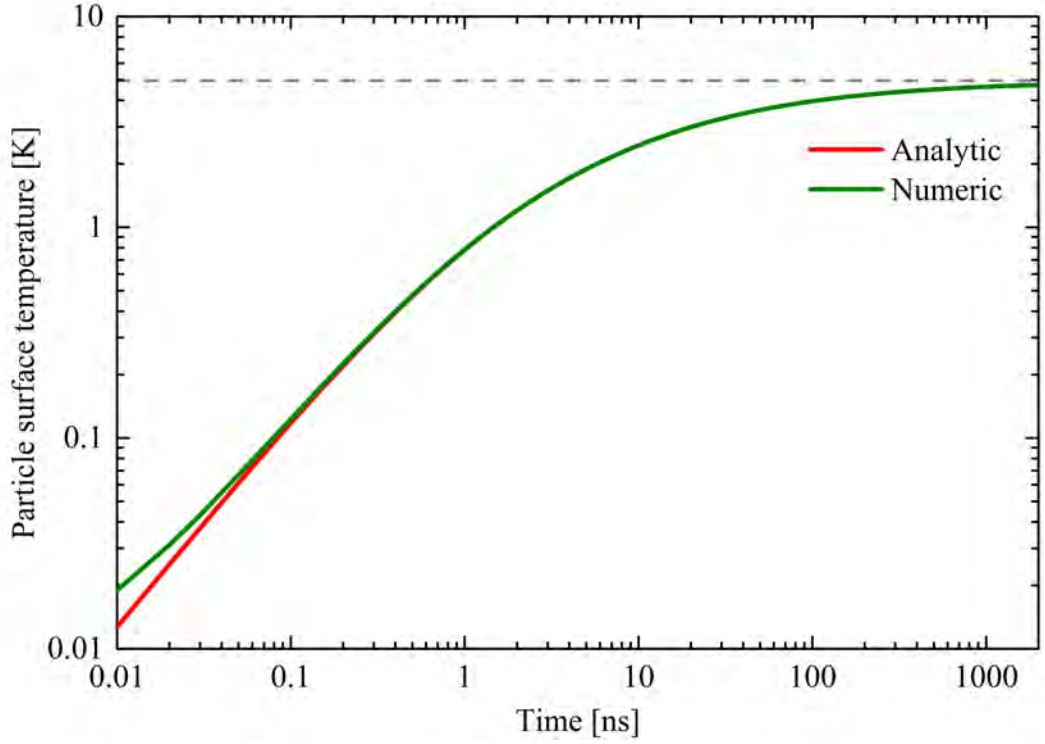

Figure 7: Numeric particle surface temperature in comparison with the analytic model, equation (30). The gray, dotted line represents the limit for large times according to equation (34).

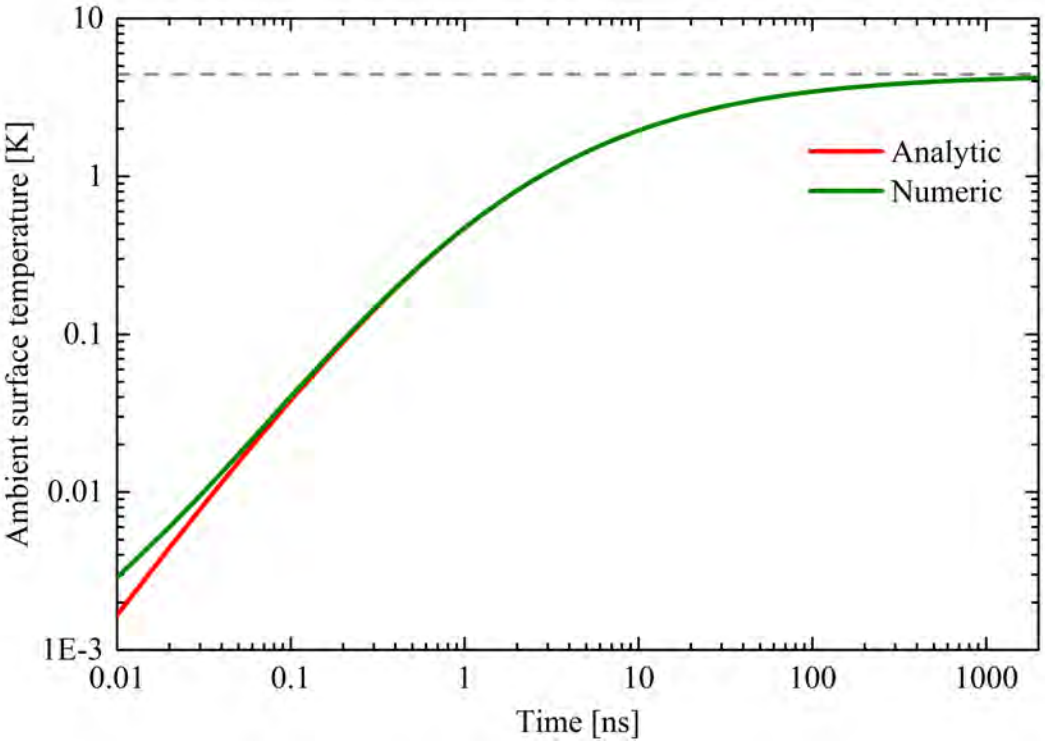

Figure 8: Numeric ambient surface temperature in comparison with the analytic model, equation (31). The gray, dotted line represents the limit for large times according to equation (33).

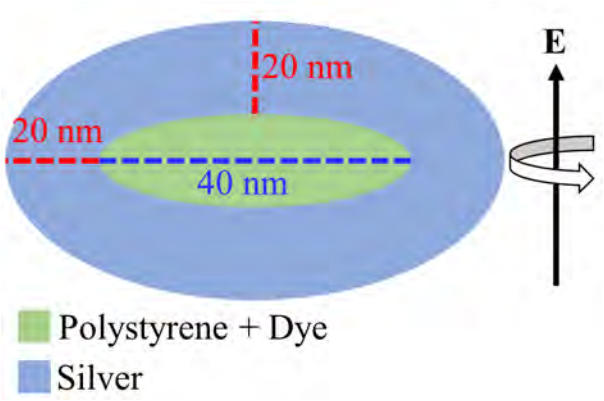

Figure 9: Oblate spheroidal geometry of a dipolar, saturated spaser. The aspect ratio of the core spheroid is 5.43. The black arrow indicates the polarization of the exciting wave, which is parallel to the axis of rotation of the oblate spheroid.

3 Heating of a spaser

3.1 Introduction

In short, a spaser is a generator of coherent local fields.[3,4] While its counterpart, the laser, produces coherent photons, a spaser generates coherent localized surface plasmons in the metal nanoparticle. However, such plasmons have a finite lifetime, their main relaxation channel being Ohmic loss (i. e. heat). This heating up of the spaser can be very intense, possibly destroying the device. Hence it is of crucial interest to understand the thermal behaviour of an operating spaser.

3.2 Finite element simulation

To model the nonlinear electrodynamic processes of a saturated spaser, I use the framework developed by Arnold et al.[19,20] I simulate a dipolar, saturated spaser surrounded by water. The structure has an oblate spheroidal geometry and consists of a gain core (host material is polystyrene) coated by a silver shell (see figure 9). The polarization of the exciting wave is parallel to the axis of rotation and the system is tuned to a spasing wavelength of 520 nm by choice of geometry.

3.2.1 Electromagnetic material properties

For the dielectric function of silver I use the data from Johnson and Christy.[16] To include a temperature dependence in the optical properties of the metal, I modify the dielectric

Name	Silver	Polystyrene	Water
Thermal conductivity	$426.4\,\mathrm{W/(m\,K)}$	$0.1556\,\mathrm{W/(m\,K)}$	$0.6056\,\mathrm{W/(m\,K)}$
Density	$10470\,\mathrm{kg/m^3}$	$1047\,\mathrm{kg/m^3}$	$997.66\,\mathrm{kg/m^3}$
Specific heat capacity	$236.66\,\mathrm{J/(kg\,K)}$	$1233\,\mathrm{J/(kg\,K)}$	$4181.5\,\mathrm{J/(kg\,K)}$

Table 3: Room temperature values for thermal material properties.[21–29]

function in the following way:

$$\varepsilon_{\mathrm{Ag}}(T) = \varepsilon_{\mathrm{Ag}}^{\mathrm{JC}} + \varepsilon_{\mathrm{Ag}}^{\mathrm{Dr}}(T) - \varepsilon_{\mathrm{Ag}}^{\mathrm{Dr}}(T_0). \tag{40}$$

Here, $\varepsilon_{\mathrm{Ag}}^{\mathrm{JC}}$ is the data from Johnson and Christy (measured at room temperature T_0) and $\varepsilon_{\mathrm{Ag}}^{\mathrm{Dr}}$ is a Drude interpolation of the data with a temperature-dependent collision frequency:

$$\varepsilon_{\mathrm{Ag}}^{\mathrm{Dr}}(T) = 1 + \chi^{\mathrm{IB}} - \frac{\omega_{\mathrm{P}}^2}{\omega(\omega + i\gamma(T))} \qquad \text{with} \qquad \gamma(T) = \gamma_0 \frac{T}{T_0}. \tag{41}$$

The parameters of the Drude interpolation are $\hbar\omega_{\mathrm{P}} = 9.222\,\mathrm{eV}$, $\hbar\gamma_0 = 0.019\,\mathrm{eV}$ and $\chi^{\mathrm{IB}} = 3.081$. To model the gain material, I use an intensity-dependent Lorentzian dielectric function,[19] which accounts for gain saturation:

$$\varepsilon_{\mathrm{G}}(s) = \varepsilon_{\mathrm{h}} - \frac{\varepsilon_{\mathrm{L}}(\omega_{\mathrm{L}} - \omega + i\gamma_{\mathrm{L}}/2)\gamma_{\mathrm{L}}/2}{(\omega_{\mathrm{L}} - \omega)^2 + (\gamma_{\mathrm{L}}/2)^2(1 + s^2)} \qquad \text{with} \qquad s = |\mathbf{E}|/E_{\mathrm{sat}} \tag{42}$$

Here, $\varepsilon_{\mathrm{h}} = 2.6$ refers to the gain host material, which is polystyrene. The other parameters of the Lorentzian are $\hbar\omega_{\mathrm{L}} = 2.391\,\mathrm{eV}$, $\hbar\gamma_{\mathrm{L}} = 1.575\,\mathrm{eV}$ and $E_{\mathrm{sat}} = 1.026 \times 10^8\,\mathrm{V/m}$. The amplitude ε_{L} of the Lorentzian increases monotonically with the pumping intensity.[19] Similar to the laser, a spaser also has a certain threshold $\varepsilon_{\mathrm{L,thr}}$ at which spasing starts. In the case considered below, the spaser operates at twice this value, i. e. $\varepsilon_{\mathrm{L}} = 2\varepsilon_{\mathrm{L,thr}} = 0.21$. The dielectric function of the surrounding water is assumed to be constant, $\varepsilon_{\mathrm{W}} = 1.78$. All materials are assumed to be non-magnetic.

3.2.2 Thermal material properties

With the exception of the Kapitza conductance, all thermal material properties are assumed to be temperature-dependent.[21–29] The values for room temperature are shown in table 3. For both the silver/polystyrene and polystyrene/water interfaces, I assume a temperate-independent Kapitza conductance of $10^8\,\mathrm{W/(m^2\,K)}$.

3.2.3 Quasistatic approximation

To estimate the spasing threshold $\varepsilon_{\mathrm{L,thr}}$ (see chapter 3.2.1), the electrodynamic response of a coated spheroid can be found in a quasistatic approximation (i. e. assuming $k \approx 0$ in the Maxwell equations). Assuming that the core, shell and the ambient have the dielectric functions ε_1, ε_2 and ε_3, the polarizability α of coated spheroid is[30]

$$\alpha = \frac{V\Big((\varepsilon_2 - \varepsilon_3)\Big(\varepsilon_2 + (\varepsilon_1 - \varepsilon_2)(L_1 - fL_2)\Big) + f\varepsilon_2(\varepsilon_1 - \varepsilon_2)\Big)}{\Big(\varepsilon_2 + (\varepsilon_1 - \varepsilon_2)(L_1 - fL_2)\Big)\Big(\varepsilon_3 + (\varepsilon_2 - \varepsilon_3)L_2\Big) + fL_2\varepsilon_2(\varepsilon_1 - \varepsilon_2)}, \tag{43}$$

where V is the total volume of the structure and $f < 1$ is the volume fraction of the core spheroid to the total structure. The function $L_i = L(e_i)$ depends on the eccentricities e_1 and e_2 of the core and shell spheroids. If both are oblate,

$$L(e) = e^{-2}\Big(1 - e^{-1}\sqrt{1 - e^2}\arcsin(e)\Big). \tag{44}$$

Using a simple model for the gain material, $\varepsilon_1 = \varepsilon_{\mathrm{h}} + i\varepsilon_{\mathrm{L,thr}}$, and Johnson-Christy data[16] for ε_2, the spasing threshold and wavelength ($\varepsilon_{\mathrm{L,thr}}$ and λ_{thr}) can be numerically calculated by setting the complex denomintor of the polarizability to zero. Figures 10 and 11 show the spasing threshold and wavelength for the geometry in figure 9 as a function of the core aspect ratio. The numerically studied spaser has an aspect ratio of 5.43, hence the quasistatic approximation yields $\varepsilon_{\mathrm{L,thr}} = 0.086$ and $\lambda_{\mathrm{thr}} = 505.8\,\mathrm{nm}$, while the numerical values are $\varepsilon_{\mathrm{L,thr}} = 0.105$ and $\lambda_{\mathrm{thr}} = 519.8\,\mathrm{nm}$. The discrepancy between the quasistatic and numerical results is due to retardation, which increases the threshold via radiative losses.

3.2.4 Heat sources and thermal limits

There are three relevant sources of heat in a spaser. The non-radiative decay of surface plasmons and the absorption of the pumping radiation generates heat in the metal component, while the non-radiative relaxation of individual dye molecules heats the gain material. In this work, I only simulate the decay of resonant surface plasmons, i. e., I assume that the intensity of non-resonant surface plasmons is negligible. I also assume that the spaser is continuously illuminated by the pump, meaning that the pumping intensity (and therefore the amplitude of the Lorentzian of the gain material, ε_{L} in equation (42)) is time-independent.

The two main factors which determine the thermal limitations of a spaser are the melting of the gain material and the sintering of the metal. Both processes would lead to structural changes on an atomic level and thus inflict irreversible damage onto the structure. While

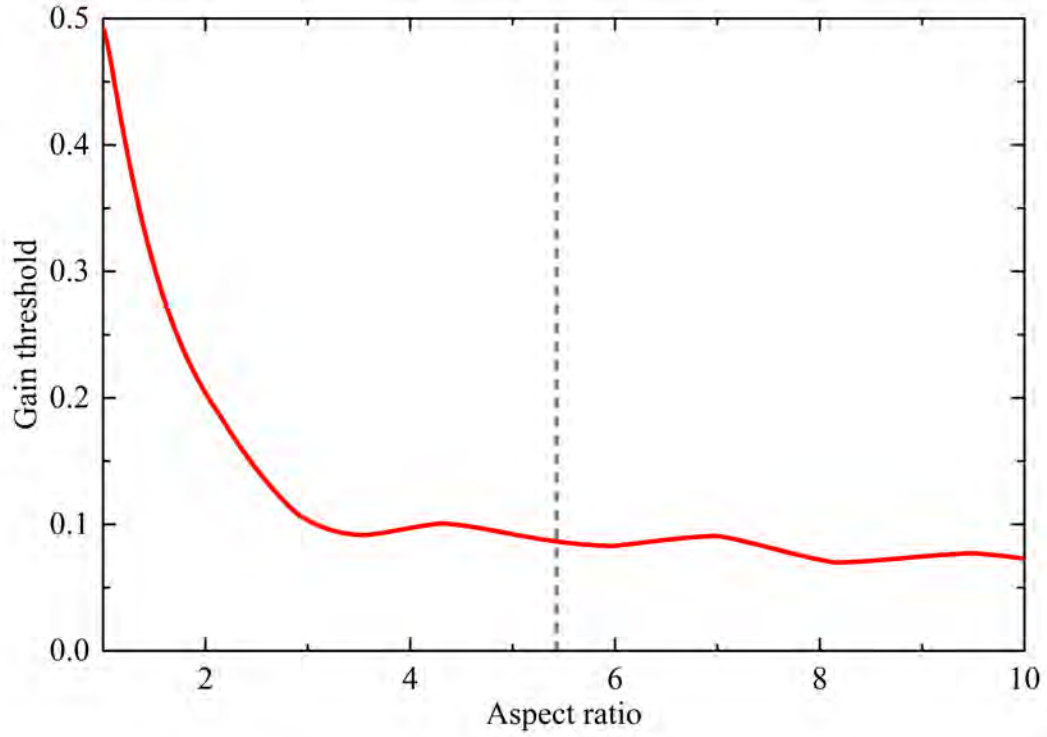

Figure 10: Quasistatic gain threshold $-\varepsilon_{\mathrm{L,thr}}$ versus the aspect ratio of the gain core for the geometry shown in figure 9. The dashed line refers to the numerically studied spaser, which has an aspect ratio of 5.43.

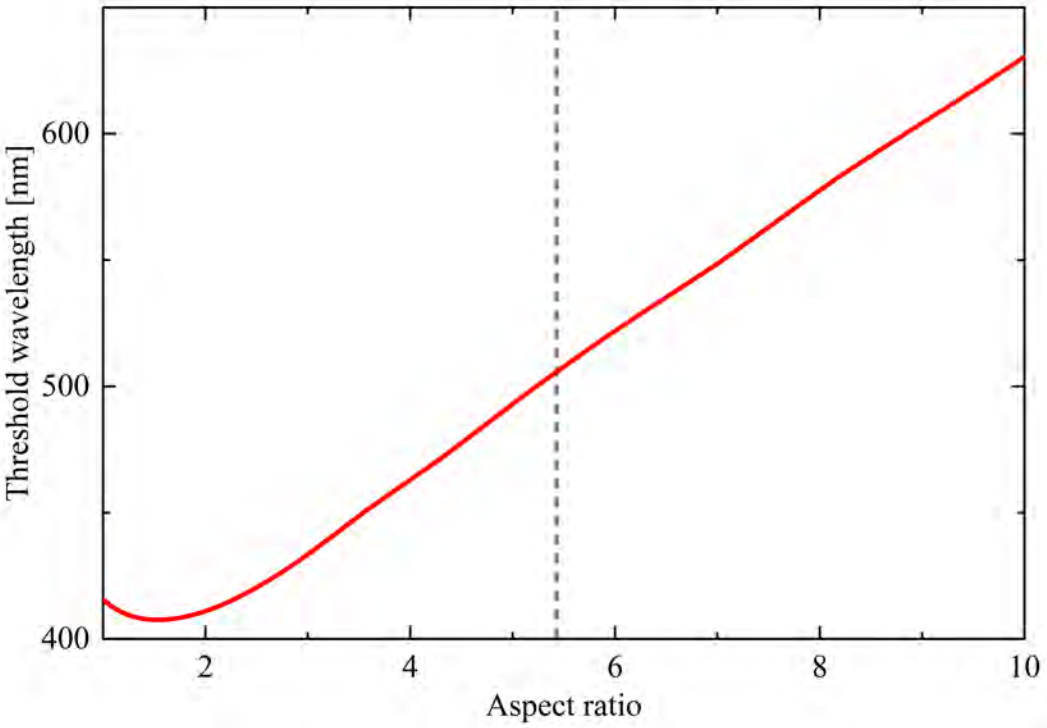

Figure 11: Quasistatic threshold wavelength λ_{thr} versus the aspect ratio of the gain core for the geometry shown in figure 9. The dashed line refers to the numerically studied spaser, which has an aspect ratio of 5.43.

the melting point of the gain material is clearly defined, the sintering of the metal is much harder to estimate. The rule of thumb is that sintering starts at approximately half the melting point temperature. The melting point of polystyrene is approximately at 510 K, while the melting point of silver is at about 1230 K. Assuming that both metal and polystyrene have similar temperature (which is reasonable given the gain-core/metal-shell geometry), the operating temperature of such a spaser should not exceed 500 K.

3.2.5 Numerical methods

The electrodynamic part is solved in frequency domain, while the thermal part is solved in time domain. However, despite the problems being set in different domains, they can still be coupled, because the electrodynamic problem equilibrates much faster than the thermal one. Hence, it is possible to couple both domains by applying the stationary electromagnetic solution from the frequency domain to every time step in the thermal problem.

Due to the dependence of the optical properties on intensity and temperature (see equations (40) and (42)), the coupled problem is nonlinear in both temperature and electric field and, as it turns out, numerically unstable. To further simplify it, I assume that the temperature inside the metal is spatially constant. This assumption is reasonable, because the thermal conductivity of the metal is 2-3 orders of magnitude higher than in the gain and surrounding materials, leading to much smaller temperature gradients in the metal nanoparticle (MNP). In addition, the heat conduction homogenizes the temperature in the MNP within several picoseconds, while the whole thermal problem takes 10 to 100 nanoseconds to reach the stationary state. Using this approximation, the electromagnetic and thermal problems then can be run separately. First, the electrodynamic problem is calculated by assuming a spatially constant temperature T in the metal for a reasonable temperature range (typically 300 K to 600 K in steps of 1 K). This is done for a fixed ε_{L}, and incident field E_{inc}. The latter is however almost irrelevant, because the field in the (generating) spaser is practically independent on E_{inc}, provided that $E_{\mathrm{inc}}/E_{\mathrm{sat}} \ll 1$. From the results I then build an average heat source $Q(T)$ inside the metal (see figure 13), which is used in the thermal simulation. Investigations of the accuracy of this method show that the difference in temperature originating from this simplification is on the order of 0.1 K and thus negligible.

3.2.6 Results

Figure 14 shows the average metal temperature of the studied spaser over time. Figure 12 shows the temperature distribution at 4 representative times. As discussed in chapter

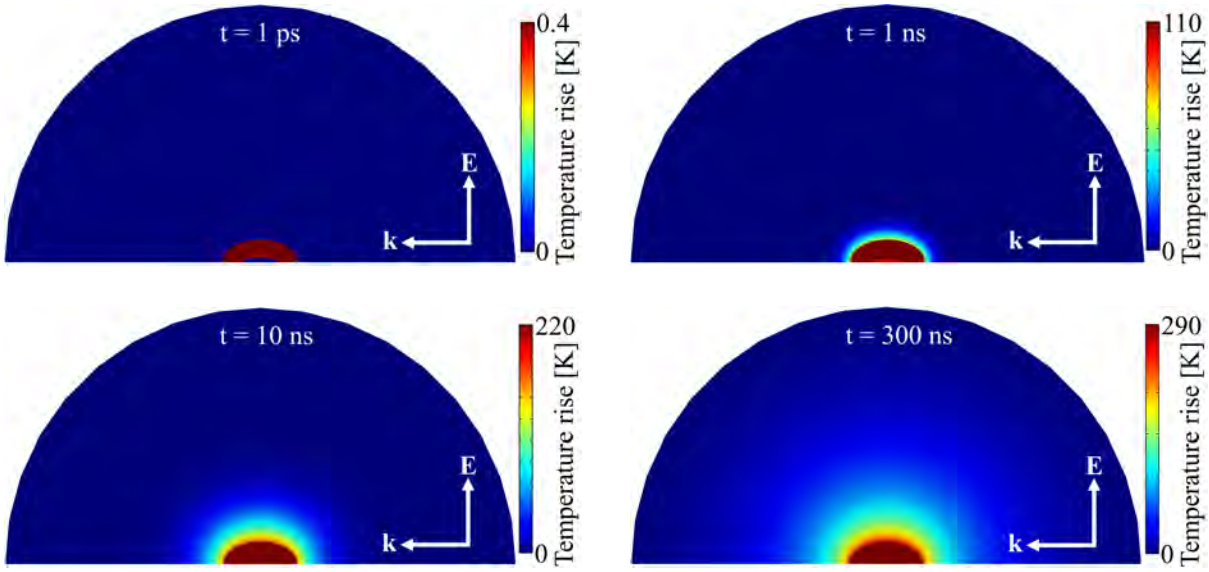

Figure 12: Spaser temperature $T - T_0$ at various times. The spaser is operating at twice the spasing threshold and a wavelength of 520 nm. The white arrows indicate the direction and polarization of the incident plane wave.

3.2.4, the operating temperature for this spaser should be below 500 K, which is clearly not the case for the stationary state of continuous pumping. To avoid permanent damage, the pump should be switched off after 2-3 ns, assuming a generous safety margin, since not all heating effects have been considered in the present simulation.

4 Summary

In chapter 2 the electromagnetic heating of a small silver particle is investigated. A simple model, which can be solved analytically, is presented, and then compared with the calculated results to verify the applied numerical methods. In chapter 3, the heating due to absorption of resonant surface plasmons in dipolar saturated spaser is simulated and estimations for its maximum safe operation time are made. In the future, the inclusion of other heating effects is planned to be able to make more quantitative predictions.

5 Acknowledgements

I would like to thank Prof. Thomas Klar, Prof. Alexander Kildishev and Dr. Nikita Arnold for providing scientific guidance. Special thanks go to Dr. Calin Hrelescu and Dr. Nikita Arnold for proofreading this paper and offering their corrections.

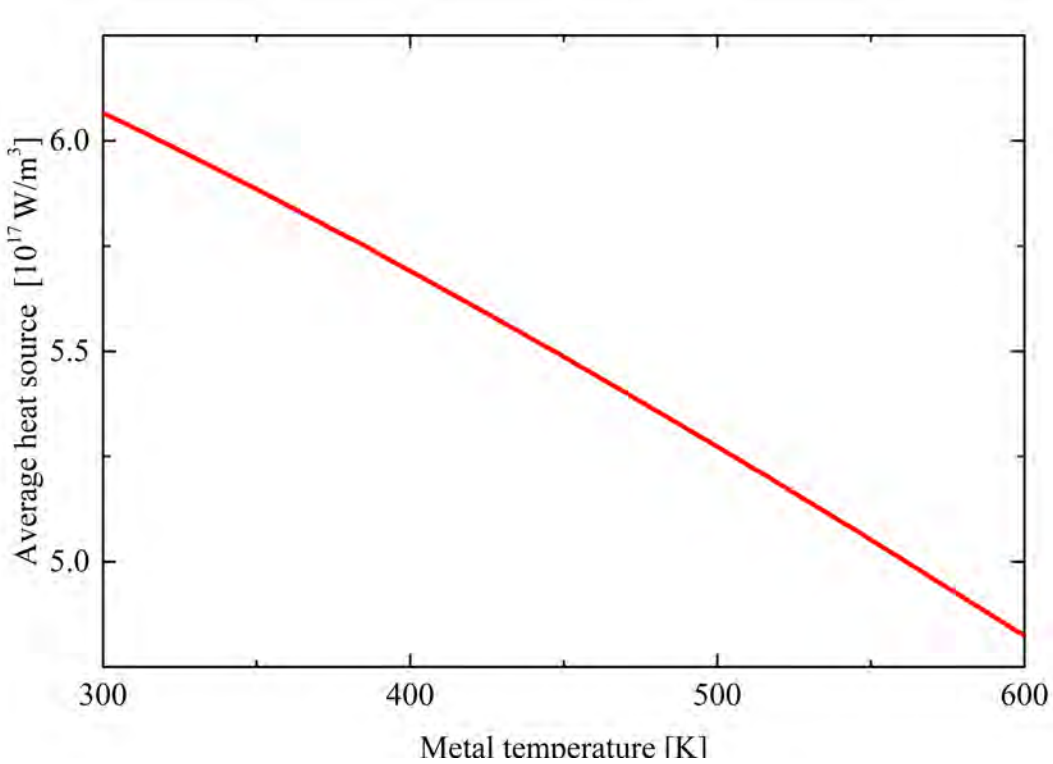

Figure 13: Average heat source versus the temperature in the metal component of the studied spaser (see figure 9). In these calculations, the metal temperature is assumed to be spatially constant.

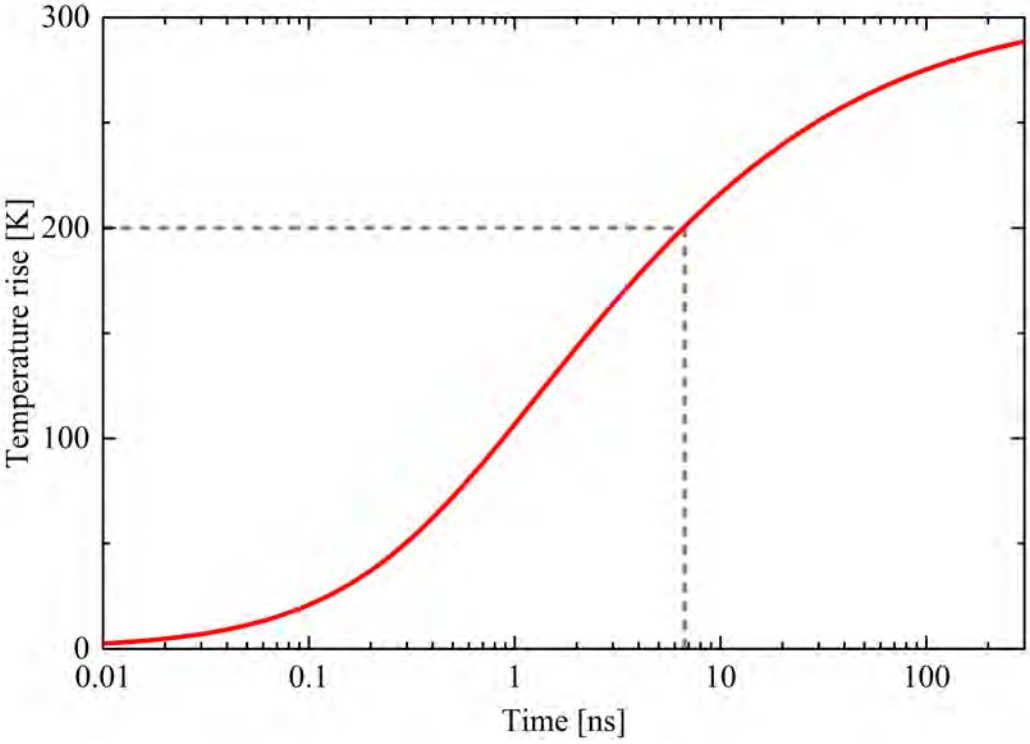

Figure 14: Average metal temperature rise $T - T_0$ of the studied spaser (see figure 9) operating at twice the spasing threshold and a wavelength of 520 nm. The dashed grey lines indicates the maximum operating temperature and corresponding pumping time, as discussed in chapters 3.2.4 and 3.2.6.

References

[1] KR Catchpole and Albert Polman. Plasmonic solar cells. *Optics express*, 16(26):21793–21800, 2008.

[2] Ananth Dodabalapur. Organic light emitting diodes. *Solid State Communications*, 102(2):259–267, 1997.

[3] Mark I Stockman. The spaser as a nanoscale quantum generator and ultrafast amplifier. *Journal of Optics*, 12(2):024004, 2010.

[4] David J Bergman and Mark I Stockman. Surface plasmon amplification by stimulated emission of radiation: Quantum generation of coherent surface plasmons in nanosystems. *Phys. Rev. Lett.*, 90(2):027402, 2003.

[5] Dakrong Pissuwan, Stella M Valenzuela, and Michael B Cortie. Therapeutic possibilities of plasmonically heated gold nanoparticles. *TRENDS in Biotechnology*, 24(2):62–67, 2006.

[6] Xi Chen, Yiting Chen, Min Yan, and Min Qiu. Nanosecond photothermal effects in plasmonic nanostructures. *ACS nano*, 6(3):2550–2557, 2012.

[7] Alexander O Govorov, Wei Zhang, Timur Skeini, Hugh Richardson, Jaebeom Lee, and Nicholas A Kotov. Gold nanoparticle ensembles as heaters and actuators: melting and collective plasmon resonances. *Nanoscale Research Letters*, 1(1):84–90, 2006.

[8] Hugh H Richardson, Zackary N Hickman, Alexander O Govorov, Alyssa C Thomas, Wei Zhang, and Martin E Kordesch. Thermooptical properties of gold nanoparticles embedded in ice: characterization of heat generation and melting. *Nano letters*, 6(4):783–788, 2006.

[9] Min Hu and Gregory V Hartland. Heat dissipation for au particles in aqueous solution: relaxation time versus size. *The Journal of Physical Chemistry B*, 106(28):7029–7033, 2002.

[10] Tatjana Stoll, Paolo Maioli, Aurélien Crut, Sergio Rodal-Cedeira, Isabel Pastoriza-Santos, Fabrice Vallée, and Natalia Del Fatti. Time-resolved investigations of the cooling dynamics of metal nanoparticles: Impact of environment. *The Journal of Physical Chemistry C*, 119(22):12757–12764, 2015.

[11] Nadine Harris, Michael J Ford, and Michael B Cortie. Optimization of plasmonic heating by gold nanospheres and nanoshells. *The Journal of Physical Chemistry B*, 110(22):10701–10707, 2006.

[12] Hugh H Richardson, Michael T Carlson, Peter J Tandler, Pedro Hernandez, and Alexander O Govorov. Experimental and theoretical studies of light-to-heat conversion and collective heating effects in metal nanoparticle solutions. *Nano letters*, 9(3):1139–1146, 2009.

[13] Ke Jiang, David A Smith, and Anatoliy Pinchuk. Size-dependent photothermal conversion efficiencies of plasmonically heated gold nanoparticles. *The Journal of Physical Chemistry C*, 117(51):27073–27080, 2013.

[14] H Goldenberg and CJ Tranter. Heat flow in an infinite medium heated by a sphere. *British Journal of Applied Physics*, 3(9):296, 1952.

[15] Pawel Keblinski, David G Cahill, Arun Bodapati, Charles R Sullivan, and T Andrew Taton. Limits of localized heating by electromagnetically excited nanoparticles. *Journal of Applied Physics*, 100(5):054305, 2006.

[16] Peter B Johnson and R-W Christy. Optical constants of the noble metals. *Physical Review B*, 6(12):4370, 1972.

[17] Gustav Mie. Beiträge zur optik trüber medien, speziell kolloidaler metallösungen. *Annalen der physik*, 330(3):377–445, 1908.

[18] COMSOL AB. COMSOL Multiphysics Reference Manual. *COMSOL Multiphysics 5.1*, 2015.

[19] Nikita Arnold, Klaus Piglmayer, Alexander V Kildishev, and Thomas A Klar. Spasers with retardation and gain saturation: electrodynamic description of fields and optical cross-sections. *Optical Materials Express*, 5(11):2546–2577, 2015.

[20] Nikita Arnold, Calin Hrelescu, and Thomas A Klar. Minimal spaser threshold within electrodynamic framework: Shape, size and modes. *Annalen der Physik*, 2015.

[21] RW Powell, Cho Yen Ho, and Peter Edward Liley. Thermal conductivity of selected materials. Technical report, DTIC Document, 1966.

[22] Lois CK Carwile and Harold J Hoge. Thermal conductivity of polystyrene: Selected values. Technical report, DTIC Document, 1966.

[23] CA Nieto de Castro, SFY Li, A Nagashima, RD Trengove, and WA Wakeham. Standard reference data for the thermal conductivity of liquids. *Journal of physical and chemical reference data*, 15(3):1073–1086, 1986.

[24] In-Kook Suh, H Ohta, and Y Waseda. High-temperature thermal expansion of six metallic elements measured by dilatation method and x-ray diffraction. *Journal of Materials Science*, 23(2):757–760, 1988.

[25] Winton Patnode and WJ Scheiber. The density, thermal expansion, vapor pressure, and refractive index of styrene, and the density and thermal expansion of polystyrene. *Journal of the American Chemical Society*, 61(12):3449–3451, 1939.

[26] Natan B Vargaftik, Yurii K Vinogradov, and Vadim S Yargin. Handbook of physical properties of liquids and gases - pure substances and mixtures. 1996.

[27] Kenneth Keith Kelley. *High-temperature heat-content, heat-capacity, and entropy data for the elements and inorganic compounds*. Number 584-585. US Govt. Print. Off., 1960.

[28] FE Karasz, HE Bair, and JM O'reilly. Thermal properties of atactic and isotactic polystyrene. *The Journal of Physical Chemistry*, 69(8):2657–2667, 1965.

[29] Milan Zábranskỳ et al. *Heat capacity of liquids: critical review and recommended values*. Amer Inst of Physics, 1996.

[30] Craig F Bohren and Donald R Huffman. *Absorption and scattering of light by small particles*. John Wiley & Sons, 2008.